

Kino-PAX: Highly Parallel Kinodynamic Sampling-based Planner

Nicolas Perrault, Qi Heng Ho, and Morteza Lahijanian

Abstract—Sampling-based motion planners (SBMPs) are effective for planning with complex kinodynamic constraints in high-dimensional spaces, but they still struggle to achieve *real-time* performance, which is mainly due to their serial computation design. We present *Kinodynamic Parallel Accelerated eXpansion (Kino-PAX)*, a novel highly parallel kinodynamic SBMP designed for parallel devices such as GPUs. *Kino-PAX* grows a tree of trajectory segments directly in parallel. Our key insight is how to decompose the iterative tree growth process into three massively parallel subroutines. *Kino-PAX* is designed to align with the parallel device execution hierarchies, through ensuring that threads are largely independent, share equal workloads, and take advantage of low-latency resources while minimizing high-latency data transfers and process synchronizations. This design results in a very efficient GPU implementation. We prove that *Kino-PAX* is probabilistically complete and analyze its scalability with compute hardware improvements. Empirical evaluations demonstrate solutions in the order of 10 ms on a desktop GPU and in the order of 100 ms on an embedded GPU, representing up to 1000 \times improvement compared to coarse-grained CPU parallelization of state-of-the-art sequential algorithms over a range of complex environments and systems.

I. INTRODUCTION

Autonomous robotic systems are increasingly deployed in dynamic environments, requiring fast, reactive motion planning that accounts for the robot's complex kinematics and dynamics. Solving the kinodynamic motion planning problem *quickly* is critical for ensuring both functionality and safety. *Sampling-based motion planners* (SBMPs) have proven effective for various difficult problems, such as complex dynamics [1]–[5], complex tasks [6]–[8], and stochastic dynamics [9]–[14]. Nevertheless, they are typically designed for serial computation, limiting their speed to CPU clock rate. While recent methods can find solutions within seconds for simple systems and tens of seconds for complex ones [1]–[3], this is insufficient for *real-time* reactivity. Given the plateau in improvements to serial computation and CPU clock speeds, parallel devices like GPUs offer promising speedups. However, current SBMP algorithms are inherently sequential and inefficient when parallelized. In this work, we aim to enable real-time motion planning for complex and high-dimensional kinodynamical systems by exploiting the parallel architecture of GPU-like devices.

In this paper, we introduce *Kino-PAX*, a highly parallel kinodynamic SBMP, designed to efficiently leverage parallel devices. *Kino-PAX* grows a tree of trajectory segments directly in parallel. Our key insight is that the iterative tree growth process can be decomposed into three massively parallel subroutines. We design *Kino-PAX* to align with the

parallel execution hierarchy of these devices, ensuring that threads are largely independent, share equal workloads, and take advantage of low-latency resources while minimizing high-latency data transfers and process synchronizations. We provide an analysis of *Kino-PAX*, showing that it is probabilistically complete. We also demonstrate, through several benchmarks, that *Kino-PAX* is robust to changes in hyperparameters and scalable to large dimensional systems.

In summary, our contributions are four-fold: (i) *Kino-PAX*, a highly parallel kinodynamic SBMP designed to leverage the parallel architecture of GPU-like devices, (ii) discussion on efficient GPU implementation of *Kino-PAX*, (iii) a thorough analysis and proof of probabilistic completeness, and (iv) benchmarks showing the efficiency and efficacy of *Kino-PAX* for complex and high-dimensional dynamical systems. Our results show that *Kino-PAX* achieves up to three-orders-of-magnitude improvement in computation time compared to our baselines, which use CPU parallelization. In all evaluated problems, *Kino-PAX* finds solutions in the order of 10 milliseconds, representing significant progress in enabling real-time kinodynamic motion planning.

A. Related Work

Geometric Motion Planning: SBMPs have a long-standing history in addressing the geometric motion planning problem, as established by foundational works such as *Probabilistic RoadMaps* (PRM) [15], *Expansive-Space Tree* (EST) [16], *Rapidly-exploring Random Tree* (RRT) [17], etc. In general terms, SBMP techniques involve finding a path from a starting configuration to a goal region by constructing a graph or tree, where nodes represent geometric configuration and straight line edges represent transitions in the configuration space. Traditionally, these algorithms operate serially on CPU devices. However, the increasing demand for rapid replanning for complex systems in unknown and dynamic environments has driven the development of parallelization methods for geometric SBMPs. These parallelized approaches have been applied to both CPU-based planners [18], [19] and GPU-based implementations [20].

Work [18] decomposes fundamental operations of geometric SBMPs, such as collision checking, forward kinematics, and nearest neighbor search, into unconventional data layouts. This approach enables parallelism without requiring specialized hardware. Work [19] proposes growing multiple trees in parallel, where information is shared between trees, improving visibility of the search space. In [20], the authors leverage GPUs to solve the geometric path planning problem by adapting *FMT** [21] for parallelized graph search, achieving orders of magnitude performance improvements over its

Authors are with the Dept. of Aerospace at University of Colorado Boulder. {firstname.lastname}@colorado.edu

serial counterpart. While these algorithms have demonstrated orders of magnitude improvement over serial implementations, they are strictly limited to geometric problems.

Kinodynamic Motion Planning: To provide dynamically feasible and collision-free trajectories for systems with complex dynamics, a kinodynamic motion planning algorithm is used, as seen in traditional serial solutions such as [1]–[5]. The details of the kinodynamic motion planning problem are formally discussed in Section II; however, in general, these algorithms are tree-based and solve the problem by sequentially randomly extending trajectories until a path from a start state to a goal region satisfying all state constraints can be followed by a sequence of trajectory segments.

To achieve fast planning times, works [3], [5] employ space discretization. Specifically, [3] constructs a graph from discrete regions and uses it as a high-level planner to guide the motion tree. However, this approach can face the *state-explosion* problem as the dimensionality of state space increases. In contrast, [5] avoids this issue by using the discrete regions to track spatial information about the sparsity of the motion tree without constructing a graph. In the design of *Kino-PAX*, we take inspirations from those planners, using discrete regions to guide the search. Similar to [5], we use these regions for spatial information to ensure scalability. However, unlike previous work, *Kino-PAX* performs these operations in parallel subroutines.

In contrast to the parallelized geometric planning solutions discussed above, parallelization for planning under the constraints of general dynamical systems is relatively understudied in the field. An approach to parallelization for the kinodynamic problem is a coarse-grained method, where multiple trees of classical sampling-based motion planners are generated in parallel, and the first solution found is returned [22]. This technique improves average-case performance [23], and is employed in Section VI to perform CPU-based parallelization as baseline. However, the inherent sequential nature of these motion planners make them inefficient for massive parallelization. In this work, we propose a novel algorithm that enables efficient application to parallel devices.

II. PROBLEM FORMULATION

Consider a robotic system operating within a bounded workspace $W \subset \mathbb{R}^d$, where $d \in \{2, 3\}$. This workspace contains a finite set of obstacles \mathcal{O} , where each obstacle $o \in \mathcal{O}$ is a closed subset of W , i.e., $o \subseteq W$. The dynamics of the robot's motion is given by

$$\dot{x}(t) = f(x(t), u(t)), \quad (1)$$

where $x(t) \in X \subset \mathbb{R}^n$ and $u(t) \in U \subset \mathbb{R}^N$ are the robot's state and control at time t , respectively, and $f : X \times U \rightarrow \mathbb{R}^n$ is the vector field. We assume that f is a Lipschitz continuous function with respect to both arguments, i.e., there exist constants $K_x, K_u > 0$ such that for all $x, x' \in X$ and $u, u' \in U$,

$$\|f(x, u) - f(x', u')\| \leq K_x \|x - x'\| + K_u \|u - u'\|.$$

In addition to motion constraints defined by the dynamics in (1) and obstacles in \mathcal{O} , we consider state constraints, e.g.,

bound on the velocity. To this end, we define the set of valid states, i.e., states at which the robot does not violate its state constraints and does not collide with an obstacle, as the constraint-free set and denote it by $X_{\text{free}} \subseteq X$. Then, given initial state $x_{\text{init}} \in X_{\text{free}}$, time duration $t_f \geq 0$, and control trajectory $u : [0, t_f] \rightarrow U$, a *state trajectory* $x : [0, t_f] \rightarrow X$ is induced, where

$$x(t) = x_{\text{init}} + \int_0^t f(x(\tau), u(\tau)) d\tau \quad \forall t \in [0, t_f]. \quad (2)$$

Trajectory x is called *valid* if, $\forall t \in [0, t_f]$, $x(t) \in X_{\text{free}}$.

In motion planning, the interest is to find a valid trajectory x that visits a given goal set $X_{\text{goal}} \subseteq X_{\text{free}}$. Therefore, by following this trajectory, the robot is able to respect all of its motion (kinodynamic) constraints, avoid collisions with obstacles, and reach its goal. In this work, we focus on kinodynamic motion planning with an emphasis on computational efficiency through parallelism.

Problem 1 (Kinodynamic Motion Planning). *Consider a robot with dynamics in (1) in workspace W consisting of obstacle set \mathcal{O} . Given an initial state $x_{\text{init}} \in X_{\text{free}} \subseteq X$ and goal region $X_{\text{goal}} \subseteq X_{\text{free}}$, efficiently find a control trajectory $u : [0, t_f] \rightarrow U$ such that its induced trajectory x through (2) is valid and reaches goal, i.e., $x(0) = x_{\text{init}}$ and*

$$\begin{aligned} x(t) &\in X_{\text{free}} & \forall t \in [0, t_f], \\ x(t) &\in X_{\text{goal}} & \exists t \in [0, t_f]. \end{aligned}$$

Note that this is a challenging problem. The simpler problem of geometric motion planning (by ignoring dynamics) is already PSPACE-complete [24], and the addition of kinodynamic constraints makes finding a solution considerably more difficult due to the increase in search space dimension and dynamic complexities [25], [26]. Existing algorithms find solutions in the order of seconds for simple (e.g., linear) systems and tens of seconds for more complex non-linear systems [1]–[3] on standard benchmark problems. When combined with the need for fast replanning in, e.g., unknown and changing environments, finding solutions in real-time (milliseconds) becomes crucial for ensuring the functionality and safety of autonomous systems.

With the availability of onboard GPUs, parallel computation provides a promising approach for finding solutions quickly. Hence, in our approach, we focus on achieving efficiency through a highly parallelizable algorithm.

III. KINO-PAX

Our approach to Problem 1 is a highly parallel algorithm that is able to exploit the many-core architecture of GPU-like processors. To achieve efficient performance on these high-throughput devices, it is crucial that our algorithm complements the execution hierarchy of such processors to optimize resource utilization. For the development of this algorithm, we follow the guidance of [27], [28] and base our development on three key principles: (i) *thread independence*, the ability for each thread in a program to execute without being dependent on the state or result of other threads; (ii) *even*

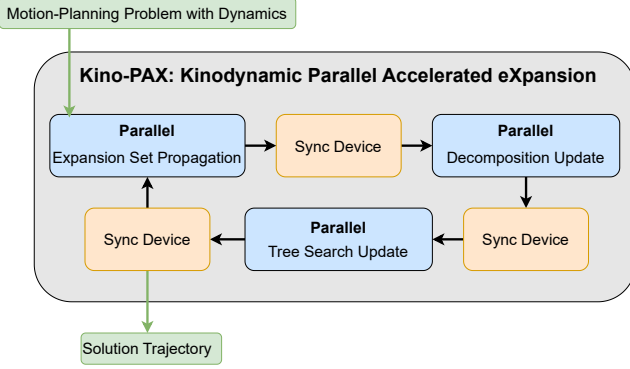


Fig. 1: Overview of *Kino-PAX*.

workloads across threads, each thread is assigned an equal or nearly equal number of operations throughout its execution; (iii) *utilization of low-latency memory*, groups of threads utilize low-latency memory to share information and reduce the number of higher-latency global memory accesses.

With these principles in mind, we introduce *Kinodynamic Parallel Accelerated eXpansion* (*Kino-PAX*), a highly parallel kinodynamic SBMP. An overview of *Kino-PAX* is shown in Fig. 1. *Kino-PAX* grows a tree of trajectory segments in parallel. This is achieved by decomposing the iterative tree growth process, i.e., selection of nodes, extension, validity checking, and adding new nodes to the tree, into three massively parallel subroutines. Each subroutine follows the key principles of *thread independence*, *balanced workloads*, and *low-latency memory utilization*. Additionally, to ensure fast and efficient planning iterations, we minimize the communication needed in the synchronization steps between subroutines, e.g., CPU-GPU communication.

At each iteration of *Kino-PAX*, a set of nodes in the tree is expanded in parallel. Each sample is extended multiple times through random sampling of controls, also in parallel. We dynamically adjust the number of extensions in each iteration to maintain an effective tree growth rate, ensuring efficient usage of the device's throughput. After extension, a new set of nodes are selected independently to be propagated in the next iteration.

To guide the search process, *Kino-PAX*, similar to [3], [5], employs a high-level space decomposition approach. We designed this method to be well-suited for parallel computation. This decomposition estimates exploration progress in each region, allowing threads to act independently when adding new nodes to the tree and identifying promising nodes for extension. As more trajectory segment data becomes available, the estimate of promising space regions is improved, allowing *Kino-PAX* to focus on propagating a large number of favorable nodes into less explored areas of the space.

A. Core Algorithm

Here, we present a detailed description of *Kino-PAX*. Pseudocode of *Kino-PAX* is presented in Alg. 1, with subroutines Algs. 2, 3, and 4, and a full planning iteration is illustrated in Fig. 4. *Kino-PAX* organizes samples into

Algorithm 1: *Kino-PAX*

Input : $x_{\text{init}}, X_{\text{goal}}, t_{\text{max}}$
Output: Solution trajectory \mathbf{x}

- 1 $\mathcal{T} \leftarrow$ Initialize tree with root node x_{init}
- 2 $V_E \leftarrow \{x_{\text{init}}\}$, $V_U, V_O \leftarrow \emptyset$
- 3 Initialize \mathcal{R} with $P_{\text{accept}}(\mathcal{R}_i) = 1$ for each $\mathcal{R}_i \in \mathcal{R}$
- 4 **while** $\text{Elapsed Time} < t_{\text{max}}$ **do**
- 5 Propagate $(V_E, V_U, \mathcal{R}, \lambda)$
- 6 UpdateEstimates (\mathcal{R})
- 7 $\mathbf{x} \leftarrow \text{UpdateNodeSets} (V_U, V_E, V_O, \mathcal{T}, \mathcal{R}, X_{\text{goal}})$
- 8 **if** $\mathbf{x} \neq \text{null}$ **then return** \mathbf{x} ;
- 9 **return** null

three distinct sets: V_U , V_O , V_E . The set V_U consists of newly generated promising samples that have not yet been added to the tree. The set V_O includes tree nodes that are not currently considered for expansion; intuitively, these nodes are located in densely populated or frequently invalid regions of the search space. Finally, V_E comprises the set of nodes that are flagged for parallel expansion. Further, *Kino-PAX* maintains the spatial search progress information using a partition of the state space denoted by \mathcal{R} .

1) *Initialization*: In Alg. 1, *Kino-PAX* takes as input the initial state x_{init} , a goal region X_{goal} , and a maximum execution time t_{max} . In Lines 1-2, a tree \mathcal{T} is initialized with x_{init} at its root. Additionally, the set V_E is initialized with the state x_{init} and the sets V_U and V_O are initialized as empty. In Line 3, the space decomposition \mathcal{R} is initialized in the state space, where the decomposition consists of non-overlapping regions, such that:

$X = \bigcup_{i=1}^n \mathcal{R}_i$ and $\forall i \neq j \in \{1, \dots, n\}$, $\text{Int}(\mathcal{R}_i) \cap \text{Int}(\mathcal{R}_j) = \emptyset$, where $\text{Int}(\mathcal{R}_i)$ is the interior of \mathcal{R}_i . Each \mathcal{R}_i is then further partitioned to a set of finer regions. We denote the k -th sub-region of \mathcal{R}_i by \mathcal{R}_i^k , i.e., $\mathcal{R}_i = \bigcup_{k=1}^{n'} \mathcal{R}_i^k$. For each region $\mathcal{R}_i \in \mathcal{R}$, several metrics are calculated to assess the exploration progress of the tree. These metrics, adapted from [3], are designed to be effective in identifying promising regions for systems with complex dynamics and are well suited for parallelism. Specifically, *Kino-PAX* updates the following metrics for each region, \mathcal{R}_i , after each iteration of parallel propagation to continually guide the search process:

- $\text{Cov}(\mathcal{R}_i)$: estimates the progress made by the tree planner in covering \mathcal{R}_i ;
- $\text{FreeVol}(\mathcal{R}_i)$: estimates the free volume of \mathcal{R}_i .

The exact expressions for $\text{Cov}(\mathcal{R}_i)$ and $\text{FreeVol}(\mathcal{R}_i)$ are the same as in [3], which we also show in Sec. III-A.3.

These metrics determine a score value, $\text{Score}(\mathcal{R}_i)$ and subsequently a probability $P_{\text{accept}}(\mathcal{R}_i)$, which aid *Kino-PAX* in adding favorable samples to \mathcal{T} and assessing if an existing node should be extended. During initialization, all $P_{\text{accept}}(\mathcal{R}_i)$ values are set to 1.

2) *Node Extension*: After initialization, the main loop of the algorithm begins (Lines 4–8). In each iteration, the Propagate (Alg. 2) function is called to propagate the

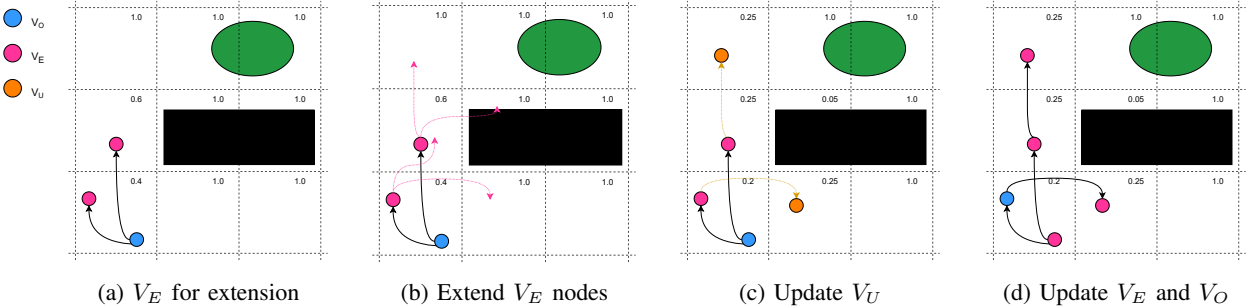


Fig. 2: Illustration of a single iteration in the *Kino-PAX* expansion process. (a) The current sets V_E and V_O , where the numbers in each grid cell represent the value of $P_{accept}(\mathcal{R}_i)$. (b) Expansion of each node in V_E with a branching factor of $\lambda = 2$. (c) Acceptance of promising samples and the update of $P_{accept}(\mathcal{R}_i)$. (d) The updated set V_E , prepared for expansion in the next iteration.

Algorithm 2: Propagate

```

Input :  $V_E, V_U, \mathcal{R}, \lambda$ 
Output: Updated  $V_U$ 
foreach  $x \in V_E$  do
  for  $i = 1, \dots, \lambda$  do
    Uniformly sample  $u$  and  $dt$  ;
     $x' \leftarrow \text{PropagateODE}(x, u, dt)$  ;
    Map  $x'$  to region  $\mathcal{R}_i^k$  ;
    if the trajectory from  $x$  to  $x'$  is valid then
      Increment  $n_{valid}(\mathcal{R}_i)$  ;
      if  $\mathcal{R}_i^k$  unvisited or with  $P_{accept}(\mathcal{R}_i)$  then
        Add  $x'$  to  $V_U$  ;
    else
      Increment  $n_{invalid}(\mathcal{R}_i)$  ;
  
```

set V_E in parallel (Line 5, Fig. 2b). Each node $x \in V_E$ is expanded $\lambda \in \mathbb{N}^+$ times using λ threads, where each thread handles one expansion of x (Alg. 2, Lines 1–2). For each thread, a control $u \in U$ and a time duration $dt \in (0, T_{prop}]$ are randomly sampled, and the node's continuous state x is propagated using dynamics in (1) to generate a new sample state x' (Alg. 2, Lines 3–4). Next, the corresponding region of x' , \mathcal{R}_i^k , is calculated (Alg. 2, Line 5). Then, in Line 6, the trajectory segment from x to x' is checked for validity, i.e., if it is in X_{free} . Throughout the trajectory segment, a user-defined collision check is performed (our implementation uses a coarse-phase bounding volume hierarchies method discussed in [20]). If the extended segment is valid, we increment the total number of valid samples in \mathcal{R}_i . Next, x' is added to the set V_U if its corresponding region \mathcal{R}_i^k is unvisited; if \mathcal{R}_i^k already contains a node, then x' is added to V_U with probability $P_{accept}(\mathcal{R}_i)$, which favors promising samples (Alg. 2, Lines 8–9, Fig. 2c). Alternatively, if the trajectory segment is invalid, we increment the count of invalid samples in \mathcal{R}_i , as shown in Line 11. This information guides future propagation iterations away from regions that are frequently invalid, improving search efficiency.

3) *Node Selection*: After all samples in V_E have been expanded, the `UpdateEstimates` (Alg. 3) subroutine is called. In this subroutine, metrics for each visited region

Algorithm 3: UpdateEstimates

```

Input :  $\mathcal{R}$ 
Output: Updated estimates for each region  $\mathcal{R}_i$ 
foreach  $\mathcal{R}_i \in \mathcal{R}_{avail}$  do
  UpdateFreeVol( $\mathcal{R}_i$ );
  UpdateCoverage( $\mathcal{R}_i$ );
  UpdateScore( $\mathcal{R}_i$ );
foreach  $\mathcal{R}_i \in \mathcal{R}_{avail}$  do
  UpdateAccept( $\mathcal{R}_i$ );

```

(i.e., a region with a node $x \in \mathcal{T}$), denoted by \mathcal{R}_{avail} , are updated in parallel, with a thread handling a unique region $\mathcal{R}_i \in \mathcal{R}_{avail}$, calculating $Cov(\mathcal{R}_i)$ and $FreeVol(\mathcal{R}_i)$ (Alg. 3, Lines 1–3). For each thread, $Cov(\mathcal{R}_i)$ is set to the number of visited sub-regions within \mathcal{R}_i , and $FreeVol(\mathcal{R}_i)$ is calculated as

$$FreeVol(\mathcal{R}_i) = \frac{(\delta + n_{valid}(\mathcal{R}_i)) \cdot vol(\mathcal{R}_i)}{\delta + n_{valid}(\mathcal{R}_i) + n_{invalid}(\mathcal{R}_i)}, \quad (3)$$

where $\delta > 0$ is a small constant, and $vol(\mathcal{R}_i)$ represents the mapped workspace volume of the region \mathcal{R}_i . Subsequently, on Line 4 of Alg. 3, each thread calculates its corresponding $Score(\mathcal{R}_i)$ value with

$$Score(\mathcal{R}_i) = \frac{FreeVol^4(\mathcal{R}_i)}{(1 + Cov(\mathcal{R}_i))(1 + (n_{valid}(\mathcal{R}_i) + n_{invalid}(\mathcal{R}_i))^2)}, \quad (4)$$

which prioritizes regions that are less visited and have a high free volume and low coverage.

Once all score values have been updated, each visited region's $P_{accept}(\mathcal{R}_i)$ probability is refined (Alg. 3 Lines 5–6, Fig. 2c). This process, again, is done in parallel with a thread being designated to a unique $\mathcal{R}_i \in \mathcal{R}_{avail}$ and $P_{accept}(\mathcal{R}_i)$ being set by

$$P_{accept}(\mathcal{R}_i) = \min \left\{ 1, \frac{Score(\mathcal{R}_i)}{\sum_{\mathcal{R}_j \in \mathcal{R}_{avail}} Score(\mathcal{R}_j)} + \epsilon \right\}, \quad (5)$$

where $0 < \epsilon \ll 1$ is a constant and $\mathcal{R}_{avail} \in \mathcal{R}$ represents the set of regions that contain a node in \mathcal{T} . We note that the expressions for the metrics in (3)–(5) are taken from [3].

Once the $P_{accept}(\mathcal{R}_i)$ probabilities have been updated for all available regions, the `UpdateNodeSets` subroutine is

Algorithm 4: UpdateNodeSets

Input : $V_U, V_E, V_O, \mathcal{T}, \mathcal{R}, X_{goal}$
Output: Trajectory if a goal is found, otherwise *null*

```

1 foreach  $x \in V_E$  do
2   | Map  $x$  to  $\mathcal{R}_i$ ;
3   | Move  $x$  to  $V_O$  with probability  $1 - P_{accept}(\mathcal{R}_i)$ ;
4 foreach  $x \in V_U$  do
5   | Move  $x$  from  $V_U$  to  $V_E$  and  $\mathcal{T}$ ;
6   | if  $x \in X_{goal}$  then return Trajectory  $x_{init}$  to  $x$  ;
7 foreach  $x \in V_O$  do
8   | Map  $x$  to  $\mathcal{R}_i$ ;
9   | Move  $x$  to  $V_E$  with probability  $P_{accept}(\mathcal{R}_i)$ ;
10 return null
```

called (Alg. 1, Line 9, Fig. 2d). In Lines 1–3 of Alg. 4, we remove samples from the expansion set V_E randomly with probability $1 - P_{accept}(\mathcal{R}_i)$, ensuring that promising samples remain in V_E . Then, we move the newly generated samples, V_U , to \mathcal{T} and add them to the expansion set V_E . If any newly generated nodes satisfy goal criteria, we return the valid trajectory \mathbf{x} (Alg. 4, Lines 4–6). Finally, we move inactive samples in V_O to the expansion set if deemed promising with the updated search information (Alg. 4, Lines 7–9).

Kino-PAX repeats the main loop of Propagate, UpdateEstimates and UpdateNodeSets until a solution trajectory \mathbf{x} that solves Problem 1 is returned, or a user-defined time limit t_{max} is surpassed.

IV. IMPLEMENTATION DISCUSSION

In this section, we discuss how *Kino-PAX* can be tuned to match a problem’s difficulty, and present the properties of *Kino-PAX* that enable efficient parallelism.

A. Tuning Parameter

In practice, due to the limitations of device memory and the high cost of vector resizing operations, we predefine the maximum size of the tree rather than constraining the runtime, similar to the approach taken in PRM. This introduces a hyperparameter for *Kino-PAX*, denoted as t_e , which we refer to as the expected tree size. Specifically, t_e corresponds to the maximum number of nodes in *Kino-PAX* and should be tuned according to the difficulty of the problem at hand.

Varying, t_e has two main effects on the performance of *Kino-PAX*. Firstly, an increase in t_e increases the branching factor λ which is updated for each iteration of parallel propagation and is set according to

$$\lambda = \min \left\{ \lambda_{max}, \left\lfloor \frac{t_e - |\mathcal{T}|}{|V_E|} \right\rfloor \right\}, \quad (6)$$

where λ_{max} is the user-defined maximum branching factor and $|\mathcal{T}|$ and $|V_E|$ are the numbers of nodes in \mathcal{T} and V_E , respectively. Eq. (6) ensures that in the early iterations, when $|\mathcal{T}|$ is much smaller than t_e , a larger λ is used. This better uses available throughput and helps accelerate the initial stages of tree propagation. As $|\mathcal{T}|$ approaches t_e

and $|V_E|$ is large, a smaller λ is used to prevent device serialization and increase tree sparsity.

Secondly, t_e affects the number of nodes that can be included in \mathcal{T} . As the problem difficulty increases, such as with a system’s state dimension, a larger t_e is recommended to sufficiently explore the space. *Kino-PAX*’s search characteristics make finding a suitable t_e relatively straightforward for a given system, as the tree expands in all accessible free space areas. We demonstrate this in Sec. VI, where systems with the same state dimension utilize a constant t_e value across all testing environments. In Sec. VI, we also show that as t_e increases, the success rate of *Kino-PAX* converges to 100%.

Remark 1. *The maximum tree size can be made adaptive by increasing t_e by a constant multiple if a solution is not found after the tree size nears its threshold. However, this introduces vector resizing operations on high latency device memory, slowing down the search.*

B. Efficient Application to Parallel Devices

Kino-PAX’s propagation subroutine implementation is well-suited for parallelism due to three main factors. First, during node expansion, we utilize low-latency on-chip memory to distribute the state $x \in V_E$ among all λ threads assigned to expand the node. Second, we minimize thread divergence by having each thread create only a single trajectory segment. Third, the acceptance of new samples and their addition to V_U is performed completely independently, using (5) and unique thread identifiers to avoid memory write conflicts.

Kino-PAX maintains its space decomposition in a parallel-friendly manner through the metrics (3)–(4) that can be calculated independently of other regions and by ensuring that each region’s calculations have an equal number of operations. Further, we avoid the need for serial data structures when choosing expansion nodes by adding samples to V_E independently via the acceptance probability (5).

Furthermore, the organization of samples into three disjoint sets, V_U , V_O , and V_E , enables a straightforward and memory-efficient representation. In *Kino-PAX*, we do this via a boolean-mask representation that is thoroughly discussed in [29]. For completeness, we also briefly describe the implementation below.

Kino-PAX’s three sets partition all samples through boolean flags, where a sample (i.e., an n -dimensional floating point representation) is stored in a one dimensional t_e -sized array, and its corresponding index in the large array is set to *true* in one of the sets. We then efficiently access the correct sample information via unique thread identifiers and a prefix-sum operation over the boolean set which essentially equates to a parallelized graph search.

Finally, we pre-allocate a large memory chunk on the GPU that can accommodate t_e nodes. This memory acts as an empty tree structure that is populated as planning progresses, eliminating the need for expensive vector resizing operations and allowing *Kino-PAX* to quickly iterate through the planning process. Additionally, this implementation

keeps all large data structures entirely on the GPU. During planning, only small pieces of data are transferred to the CPU, reducing idle time between subroutine calls.

V. ANALYSIS

Here, we show that *Kino-PAX* is probabilistically complete for Problem 1 and analyze its scalability.

A. Probabilistic Completeness

We begin with a definition of probabilistic completeness for algorithms that solve Problem 1.

Definition 1 (Probabilistic Completeness). *A sampling-based algorithm is probabilistically complete if the probability that the algorithm fails to return a solution, given one exists, approaches zero as the number of samples approaches infinity.*

We first show that, in *Kino-PAX*, every tree node has a non-zero probability of being extended.

Lemma 1. *Let $x \in \mathcal{T}$ be a node in the tree. The probability that x is selected for extension is lower bounded by $\epsilon \in (0, 1)$.*

Proof. The probability of extending a node $x \in \mathcal{T}$ in *Kino-PAX* is calculated using (5) for its corresponding region $\mathcal{R}_i \in \mathcal{R}$. We demonstrate that every region \mathcal{R}_i falls into one of three cases, and in each case, (5) is lower bounded by ϵ .

Case 1: a region \mathcal{R}_i is entirely in invalid space, i.e., $\mathcal{R}_i \cap X_{\text{free}} = \emptyset$, meaning \mathcal{R}_i cannot contain a tree node and $\mathcal{R}_i \notin \mathcal{R}_{\text{avail}}$. Thus, (5) is set to $1 > \epsilon$, as per Line 3 of Alg. 1.

Case 2: a region \mathcal{R}_i is entirely within free space, i.e., $\mathcal{R}_i \subseteq X_{\text{free}}$. If \mathcal{T} does not contain a node in \mathcal{R}_i , then $\mathcal{R}_i \notin \mathcal{R}_{\text{avail}}$, and (5) is set to $1 > \epsilon$, as by Line 3 of Alg. 1. However, if \mathcal{T} does contain a node in \mathcal{R}_i , we examine the worst-case scenario that produces the lowest probability from (5). In this scenario, the number of nodes in \mathcal{R}_i approaches infinity, driving the score of \mathcal{R}_i to 0 by (4). Additionally, in a worst-case scenario, the score of all other available regions approaches infinity. In this case, (5) trivially approaches ϵ .

Case 3: \mathcal{R}_i is partially in X_{free} , i.e., $\mathcal{R}_i \cap X_{\text{free}} \neq \emptyset$ and $\mathcal{R}_i \cap X_{\text{free}} \neq \mathcal{R}_i$. In this case, similar to above, if $\mathcal{R}_i \notin \mathcal{R}_{\text{avail}}$, (5) is set to 1 by Line 3 of Alg. 1. If $\mathcal{R}_i \in \mathcal{R}_{\text{avail}}$, as in *Case 2*, (5) approaches ϵ in the worst-case, when the number of nodes in \mathcal{R}_i approaches infinity. \square

Finally, we can state our main analysis result.

Theorem 1. *Kino-PAX is probabilistically complete.*

Proof Sketch. Our proof is an adaptation of the result from [30], originally established for kinodynamic RRT, for *Kino-PAX*. Specifically, the conditions laid out in [30, Lemma 2-3] hold under the assumptions of Problem 1 in this paper. Furthermore, Lemma 1 provides a lower bound $\epsilon > 0$ on the probability of extending from an arbitrary tree node. By combining [30, Lemma 2-3] with Lemma 1, we can follow the same logical structure as the proof of [30, Theorem 2]. Thus, as the number of samples approaches infinity, *Kino-PAX* asymptotically almost-surely finds a valid trajectory from x_{init} to X_{goal} that solves Problem 1. \square

B. Scalability

Here, we discuss the scalability of *Kino-PAX*. Firstly, *Kino-PAX*'s scalability increases as the number of cores in the parallel device increases. Since *Kino-PAX* supports adaptive tuning of the branching factor λ through varying t_e , an increased number of cores can be leveraged by increasing t_e and setting a higher λ_{max} . This results in computation time improvements as the number of cores increase, allowing *Kino-PAX* to scale as parallel hardware computation power improves.

Secondly, as the problem becomes more complex, i.e., requiring a larger tree (more nodes) to find a solution, traditional tree-based SBMPs suffer. That is, they slow down significantly as the number of nodes increases due to the sequential nature of those algorithms. However, *Kino-PAX* does not struggle with increasing number of nodes, unless the tree size nears its threshold and a resizing operation is needed. This property makes *Kino-PAX* particularly more advantageous for planning for systems with large dimensional state spaces since they often require large trees to sufficiently search the space.

VI. EXPERIMENTS

We demonstrate the performance of *Kino-PAX* in planning for various dynamical systems across three 3D environments shown in Fig. 4. The considered systems are: (i) 6D double integrator, (ii) 6D Dubins airplane [31], and (iii) 12D highly nonlinear quadcopter [32].

For each pair of dynamical system and environment, we benchmark the performance and scalability of *Kino-PAX* against four traditional SBMPs: RRT [1], EST [16], PDST [4] and SyCLOP [3]. To ensure fairness, for these comparison planners, we used a coarse-grained CPU parallelization method where multiple trees grow in parallel as suggested by [22]. Each tree is managed by a separate thread, and the planner returns the first solution found.

We implemented *Kino-PAX* in CUDA C and performed benchmarks on two GPUs with different capabilities. We used an NVIDIA RTX 4090 as a baseline, which has 16,384 CUDA cores and 24 GB of RAM. Further, to test the efficiency of *Kino-PAX* on an embedded GPU, we ran benchmarks on an NVIDIA Jetson Orin Nano,

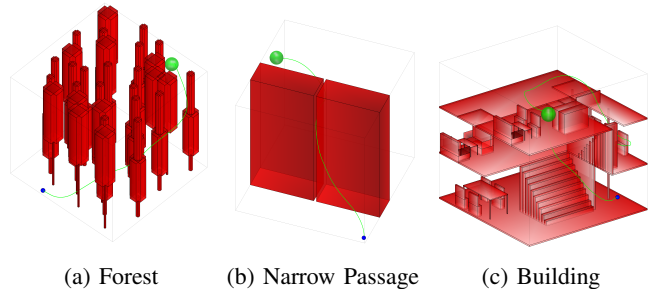


Fig. 3: Environments used throughout the experiments with the solution trajectory produced by *Kino-PAX*. Initial position and goal region are shown by blue and green spheres, respectively. Environments (a) and (c) are taken from [20].

TABLE I: Benchmark results over 50 trials with maximum planning time of 60 seconds.

Algorithm	Device	Environment 1			Environment 2			Environment 3		
		Time (ms)	$t_{alg}/t_{Kino-PAX}$	Succ %	Time (ms)	$t_{alg}/t_{Kino-PAX}$	Succ %	Time (ms)	$t_{alg}/t_{Kino-PAX}$	Succ %
6D Double Integrator										
RRT	CPU	157.0	42.0	100.0	598.1	184.1	100.0	993.7	183.4	100.0
EST	CPU	416.1	111.4	100.0	1822.5	561	100.0	5122.8	945.5	100.0
PDST	CPU	486.0	130.1	100.0	1144.7	352.4	100.0	2094.5	386.6	100.0
SyCLOP	CPU	216.6	58.0	100.0	168.1	51.8	100.0	1183.3	218.4	100.0
<i>Kino-PAX</i>	Embd. GPU	62.3	16.7	100.0	29.1	9.0	100.0	78.6	14.5	100.0
<i>Kino-PAX</i>	GPU	3.7	1.0	100.0	3.3	1.0	100.0	5.4	1.0	100.0
Dubins Airplane										
RRT	CPU	632.5	165.0	100.0	4973.9	1389.9	100.0	22698.7	3207.4	98.0
EST	CPU	275.7	71.9	100.0	3443.6	962.3	100.0	9108.5	1287.1	100.0
PDST	CPU	515.6	134.5	100.0	12410.3	3467.9	98.0	18570.2	2624.0	100.0
SyCLOP	CPU	234.4	61.2	100.0	936.2	261.6	100.0	25544.7	3610.0	100.0
<i>Kino-PAX</i>	Embd. GPU	67.5	17.6	100.0	43.1	12.0	100.0	110.5	15.6	100.0
<i>Kino-PAX</i>	GPU	3.8	1.0	100.0	3.6	1.0	100.0	7.1	1.0	100.0
12D Non Linear Quadcopter										
RRT	CPU	40694.7	2262.5	72.0	91023.1	5306.9	12.0	93144.7	3873.2	8.0
EST	CPU	10034.4	557.9	100.0	35435.9	2066	90.0	41381.0	1720.8	84.0
PDST	CPU	23726.9	1319.1	92.0	51203.4	2985.3	70.0	53169.8	2211	68.0
SyCLOP	CPU	3384.2	188.2	100.0	10181.6	593.6	100.0	86558.3	3599.4	16.0
<i>Kino-PAX</i>	Embd. GPU	797.0	44.3	100.0	681.8	39.8	100.0	935.7	38.9	100.0
<i>Kino-PAX</i>	GPU	18.0	1.0	100.0	17.2	1.0	100.0	24.1	1.0	100.0

which has 1,024 cores and 8 GB of RAM. The comparison algorithms, are implemented in C++ using *OMPL* [33] and executed on an Intel Core i9-14900K CPU with 24 cores, a base clock speed of 4.4 GHz, and 128 GB of RAM. Our implementation of *Kino-PAX* is publicly available: <https://github.com/aria-systems-group/Kino-PAX>.

We followed the standard setup configurations for all comparison algorithms as recommended by the *OMPL* documentation. All algorithms, including *Kino-PAX*, were configured to use the same methods for state propagation, state validity checking and space decomposition. For all experiments, a grid-based decomposition was used with the dimensionality of the grid equal to the system’s state-space dimension. For *Kino-PAX*’s hyperparameters, λ_{max} was set to 32 and t_e was set to 2×10^5 for all 6D systems and 4×10^5 for the 12D system. For each combination of algorithm, dynamic model, and workspace, we performed 50 queries, each with a maximum runtime of 60 seconds.

A. Benchmark Results

Table I shows the mean runtime, the speed ratio relative to the desktop GPU implementation of *Kino-PAX*, and the success rate within the allotted planning time for each combination of algorithm, environment, and dynamics.

For both 6D systems, *Kino-PAX* finds a solution trajectory in less than 8 ms across all testing environments. For the 6D Double Integrator, *Kino-PAX* is on average $85\times$, $287\times$, $433\times$ faster in Environments 1, 2, 3, respectively, compared to the baseline algorithms. For the Dubins Airplane system, the performance gap of *Kino-PAX* widens further. For instance, in Environment 3, *Kino-PAX* experiences a slowdown of less than $1.3\times$ (~ 2 ms) compared to RRT’s $22\times$ ($\sim 20,000$ ms), EST’s $1.8\times$ ($\sim 4,000$ ms), PDST’s $8.9\times$ ($\sim 16,000$ ms), and SyCLOP’s $22\times$ ($\sim 24,000$ ms). Additionally, the embedded GPU implementation of *Kino-PAX* outperforms all serial baseline methods, finding valid trajectories for all 6D problems in under 115 ms. When

dealing with the more challenging 12D nonlinear quadcopter problem, *Kino-PAX* finds solutions in less than 25 ms across all environments. On average, this marks an improvement of *three orders of magnitude* over all reference serial solutions. In the most challenging environment (Environment 3), the best-performing baseline algorithm (EST) is $1720\times$ slower than the desktop implementation of *Kino-PAX* and $44\times$ slower than the embedded GPU implementation.

As evident from the results, *Kino-PAX* outperforms baseline algorithms more significantly as the problem becomes more challenging; in other words, the performance gap significantly widens in favor of *Kino-PAX*. This is due to two main factors. First, as the dimensionality of the search space increases, exponentially more trajectory segments are required to find a valid solution. This suits *Kino-PAX* particularly well, as it is designed to propagate a massive number of nodes efficiently in parallel. Second, as the problem difficulty increases, the efficiency of *Kino-PAX* becomes more prominent. This is because unlike traditional tree-based SBMPs that slow down as the number of samples increases, *Kino-PAX* does not suffer as much with the size of the tree.

B. Effects Of Tuning Parameter t_e

To support the point made in Sec. IV that *Kino-PAX*’s hyperparameter t_e is easy to tune and that *Kino-PAX* remains efficient across a wide range of values, we present a numerical experiment showing that as *Kino-PAX* is provided with a sufficiently large t_e , its failure rate converges to zero. We also examine the impact on runtime as t_e increases. Fig. 4 presents the results for planning with the 12D nonlinear quadcopter system in Environment 1.

As shown in Fig. 4a, for small values of t_e , *Kino-PAX* is unable to find solutions, indicating that the number of samples required exceeds t_e . As t_e increases beyond 2.8×10^5 , *Kino-PAX* achieves a 100% success rate, demonstrating that t_e is not a sensitive tuning parameter with respect to finding solutions.

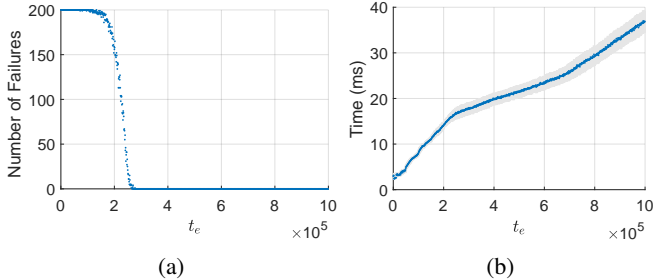


Fig. 4: Results of varying the expected tree size t_e for the 12D nonlinear quadcopter system in environment 3a. (a) Number of Failures vs. t_e . (b) Mean runtime and variance of *Kino-PAX* vs. t_e .

Fig. 4b shows an increase in the hyperparameter t_e also increases the runtime. This can be attributed to two main factors. First, as t_e increases, *Kino-PAX* typically uses a larger branching factor λ , resulting in a tree with more nodes. In this experiment, the number of nodes in the tree increases by approximately 1×10^5 for every 2×10^5 increase in t_e . Specifically, we observed 3.1×10^5 nodes when $t_e = 4 \times 10^5$ and 6.1×10^5 nodes when $t_e = 10 \times 10^5$. Second, the larger t_e demands more memory, leading to more frequent cache misses in the implementation of *Kino-PAX*, which causes data to be fetched from slower global memory more often.

VII. CONCLUSION

We have introduced a novel motion planning algorithm for kinodynamic systems that enables a significant parallelization of a process previously considered inherently sequential. Our algorithm is well suited to exploit the recent advancements of modern computing devices and is equipped to scale as hardware continues to improve. Benchmark results show planning times of less than 8 ms for 6-dimensional systems and less than 25 ms for a 12-dimensional nonlinear system, representing an improvement of up to three orders of magnitude compared to traditional motion planning algorithms. For future work, we plan to make the hyperparameter t_e dynamic (adaptive) and extend *Kino-PAX* to a near-optimal planner.

REFERENCES

- [1] S. M. LaValle and J. J. Kuffner Jr, “Randomized kinodynamic planning,” *Int. J. of robotics research*, vol. 20, no. 5, pp. 378–400, 2001.
- [2] J. M. Phillips, N. Bedrossian, and L. E. Kavraki, “Guided expansive spaces trees: A search strategy for motion-and cost-constrained state spaces,” in *Int'l Conf. on Robotics and Automation*, vol. 4. IEEE, 2004, pp. 3968–3973.
- [3] E. Plaku, L. E. Kavraki, and M. Y. Vardi, “Motion planning with dynamics by a synergistic combination of layers of planning,” *IEEE Transactions on Robotics*, vol. 26, no. 3, pp. 469–482, 2010.
- [4] A. M. Ladd and L. E. Kavraki, “Fast tree-based exploration of state space for robots with dynamics,” *Algorithmic Foundations of Robotics VI*, pp. 297–312, 2005.
- [5] I. A. Sucan and L. E. Kavraki, “A sampling-based tree planner for systems with complex dynamics,” *IEEE Transactions on Robotics*, vol. 28, no. 1, pp. 116–131, 2011.
- [6] A. Bhatia, L. E. Kavraki, and M. Y. Vardi, “Sampling-based motion planning with temporal goals,” in *Int'l Conf. on Robotics and Automation*. IEEE, 2010, pp. 2689–2696.
- [7] M. R. Maly, M. Lahijanian, L. E. Kavraki, H. Kress-Gazit, and M. Y. Vardi, “Iterative temporal motion planning for hybrid systems in partially unknown environments,” in *Hybrid Systems: Computation and Control*. Philadelphia, PA: ACM, Apr. 2013, pp. 353–362.
- [8] M. Lahijanian, M. R. Maly, D. Fried, L. E. Kavraki, H. Kress-Gazit, and M. Y. Vardi, “Iterative temporal planning in uncertain environments with partial satisfaction guarantees,” *IEEE Transactions on Robotics*, vol. 32, no. 3, pp. 538–599, May 2016.
- [9] B. Luders, M. Kothari, and J. How, “Chance constrained rrt for probabilistic robustness to environmental uncertainty,” in *AIAA guidance, navigation, and control conference*, 2010, p. 8160.
- [10] V. A. Huynh, S. Karaman, and E. Frazzoli, “An incremental sampling-based algorithm for stochastic optimal control,” in *Int'l Conf. on Robotics and Automation*. IEEE, 2012, pp. 2865–2872.
- [11] R. Luna, M. Lahijanian, M. Moll, and L. E. Kavraki, “Optimal and efficient stochastic motion planning in partially-known environments,” in *Artificial Intelligence*. Quebec City: AAAI, 2014, pp. 2549–2555.
- [12] ———, “Asymptotically optimal stochastic motion planning with temporal goals,” in *Int'l Workshop on the Alg. Found. of Robotics*, vol. 107. Springer, Aug. 2015, pp. 335–352.
- [13] Q. H. Ho, Z. Sunberg, and M. Lahijanian, “Gaussian belief trees for chance constrained asymptotically optimal motion planning,” in *Int'l Conf. on Robotics and Automation*. IEEE, May 2022.
- [14] Q. H. Ho, Z. N. Sunberg, and M. Lahijanian, “Planning with SiMBA: Motion planning under uncertainty for temporal goals using simplified belief guides,” in *Int'l Conf. on Robotics and Automation*. London, UK: IEEE, 2023, pp. 5723–5729.
- [15] L. E. Kavraki, P. Svestka, J.-C. Latombe, and M. H. Overmars, “Probabilistic roadmaps for path planning in high-dimensional configuration spaces,” *IEEE transactions on Robotics and Automation*, vol. 12, no. 4, pp. 566–580, 1996.
- [16] D. Hsu, J.-C. Latombe, and R. Motwani, “Path planning in expansive configuration spaces,” in *Proceedings of international conference on robotics and automation*, vol. 3. IEEE, 1997, pp. 2719–2726.
- [17] S. M. LaValle and J. J. Kuffner, “Rapidly-exploring random trees: Progress and prospects,” *Alg. and comp. robotics*, pp. 303–307, 2001.
- [18] W. Thomason, Z. Kingston, and L. E. Kavraki, “Motions in microseconds via vectorized sampling-based planning,” in *Int'l Conf. on Robotics and Automation*. IEEE, 2024, pp. 8749–8756.
- [19] M. Otte and N. Correll, “C-forest: Parallel shortest path planning with superlinear speedup,” *IEEE Transactions on Robotics*, vol. 29, no. 3, pp. 798–806, 2013.
- [20] B. Ichter, E. Schmerling, and M. Pavone, “Group marching tree: Sampling-based approximately optimal motion planning on gpus,” in *Int'l Conf. on Robotic Computing*. IEEE, 2017, pp. 219–226.
- [21] L. Janson, E. Schmerling, A. Clark, and M. Pavone, “Fast marching tree: A fast marching sampling-based method for optimal motion planning in many dimensions,” *Journal of Robotics Research*, vol. 34, no. 7, pp. 883–921, 2015.
- [22] S. Caselli and M. Reggiani, “Randomized motion planning on parallel and distributed architectures,” in *Euromicro Workshop on Parallel and Distributed Processing*, 1999, pp. 297–304.
- [23] N. A. Wedge and M. S. Branicky, “On heavy-tailed runtimes and restarts in rapidly-exploring random trees,” in *Artificial Intelligence*, 2008, pp. 127–133.
- [24] J. H. Reif, “Complexity of the mover's problem and generalizations,” in *Symp. on Foundations of Comp. Science*. IEEE, 1979, pp. 421–427.
- [25] B. Donald, P. Xavier, J. Canny, and J. Reif, “Kinodynamic motion planning,” *Journal of the ACM*, vol. 40, no. 5, pp. 1048–1066, 1993.
- [26] J.-P. Laumond, “Controllability of a multibody mobile robot,” *IEEE Trans. on Robotics and Automation*, vol. 9, no. 6, pp. 755–763, 1993.
- [27] D. B. Kirk and W. H. Wen-Mei, *Programming massively parallel processors: a hands-on approach*. Morgan kaufmann, 2016.
- [28] D. Guide, “Cuda c++ programming guide,” *NVIDIA*, July, 2020.
- [29] D. Merrill, M. Garland, and A. Grimshaw, “Scalable gpu graph traversal,” *ACM Sigplan Notices*, vol. 47, no. 8, pp. 117–128, 2012.
- [30] M. Kleinbort, K. Solovey, Z. Littlefield, K. E. Bekris, and D. Halperin, “Probabilistic completeness of rrt for geometric and kinodynamic planning with forward propagation,” *IEEE Robotics and Automation Letters*, vol. 4, no. 2, pp. i–vii, 2018.
- [31] H. Chitsaz and S. M. LaValle, “Time-optimal paths for a dubins airplane,” in *2007 46th IEEE conference on decision and control*. IEEE, 2007, pp. 2379–2384.
- [32] B. Etkin and L. D. Reid, *Dynamics of flight: stability and control*. John Wiley & Sons, 1995.
- [33] I. A. Sucan, M. Moll, and L. E. Kavraki, “The Open Motion Planning Library,” *IEEE Robotics & Automation Magazine*, vol. 19, no. 4, pp. 72–82, December 2012, <https://ompl.kavrakilab.org>.